Bull. Korean Math. Soc. **54** (2017), No. 1, pp. 145–158
https://doi.org/10.4134/BKMS.b150980
pISSN: 1015-8634 / eISSN: 2234-3016

AN UNCONDITIONALLY GRADIENT STABLE NUMERICAL METHOD FOR THE OHTA–KAWASAKI MODEL

Junseok Kim and Jaemin Shin

Abstract. We present a finite difference method for solving the Ohta–Kawasaki model, representing a model of mesoscopic phase separation for the block copolymer. The numerical methods for solving the Ohta–Kawasaki model need to inherit the mass conservation and energy dissipation properties. We prove these characteristic properties and solvability and unconditionally gradient stability of the scheme by using Hessian matrices of a discrete functional. We present numerical results that validate the mass conservation, and energy dissipation, and unconditional stability of the method.

1. Introduction

We consider a diblock copolymer consisting of two homopolymer blocks A and B. The order parameter $\phi(\mathbf{x}) = \rho_A(\mathbf{x}) - \rho_B(\mathbf{x})$ is defined as the difference between the local volume fractions of A and B at the point $\mathbf{x}$. Below a critical temperature, two sequences are incompatible and the copolymer melt undergoes a spatial segregation. On the mesoscopic scale, the phase separation occurs where the microdomains of A-rich and B-rich regions emerge. The Ohta–Kawasaki model [21, 22] is

$$\phi_t(\mathbf{x},t) = \Delta\mu(\mathbf{x},t) - \alpha(\phi(\mathbf{x},t) - \bar{\phi}), \tag{1}$$

$$\mu(\mathbf{x},t) = F'(\phi(\mathbf{x},t)) - \epsilon^2\Delta\phi(\mathbf{x},t), \tag{2}$$

where $\Omega \subset \mathbb{R}^d$ $(d = 1, 2, 3)$ is a domain, $\bar{\phi} = \int_\Omega \phi(\mathbf{x},t)d\mathbf{x} / \int_\Omega d\mathbf{x}$ is the average concentration, $F(\phi) = (\phi^2-1)^2/4$ is the Helmholtz free energy, ϵ is the gradient energy coefficient related to the interfacial thickness, and α is inversely proportional to the square of the total chain length of the copolymer. The periodic

Received November 27, 2015; Revised September 22, 2016.
2010 *Mathematics Subject Classification.* Primary 65M06, 65M55.
Key words and phrases. block-copolymer, Ohta–Kawasaki model, solvability, unconditionally gradient stability.
The first author was supported by the National Research Foundation of Korea (NRF) grant funded by the Korea government (MSIP) (NRF-2014R1A2A2A01003683). The second author was supported by Basic Science Research Program through the National Research Foundation of Korea (NRF) funded by the Ministry of Education (2009-0093827).

boundary conditions are considered for ϕ and μ, because the equilibrium states of block copolymers prefer periodic structures such as spherical, cylindrical, gyroid, and lamellar [3].

Various numerical methods for solving the Ohta–Kawasaki model have been studied [1, 7, 16]. For the other numerical approach to simulate the block copolymer, we can refer the dynamic mean field theory [9], based on the self-consistent field theory. In soft materials science, these numerical methods have been used to study the phenomenological structure of the copolymer [23, 24].

Note that if $\alpha = 0$, Eq. (1) is the Cahn–Hilliard equation. The Cahn–Hilliard equation is a diffuse interface model for describing the spinodal decomposition in binary alloys [5]. Various numerical schemes [2, 6, 10, 11, 12, 13, 14, 15, 17] have been used to solve the Cahn–Hilliard equation. Among them, an unconditionally stable scheme [11, 12] were introduced by the convex-concave splitting of the nonconvex free energy as $F(\phi) = F_c(\phi) - F_e(\phi)$. The convex parts $F_c'(\phi)$ is treated implicitly and the concave part $F_e'(\phi)$ is treated explicitly. The main purpose of this paper is applying the nonlinear splitting method [11, 12] to the Ohta–Kawasaki model and proving the mass conservation and energy dissipation properties and its solvability and stability.

We now briefly review a free energy functional of nonlocal type which is considered to describe the phase separation of diblock copolymer. The free energy functional $\mathcal{E}(\phi)$ is represented as the sum of two parts as $\mathcal{E}(\phi) = \mathcal{E}_s(\phi) + \mathcal{E}_l(\phi)$. $\mathcal{E}_s(\phi)$ denotes the short-range part of $\mathcal{E}(\phi)$

$$\mathcal{E}_s(\phi) = \int_\Omega \left(F(\phi) + \frac{\epsilon^2}{2} |\nabla \phi|^2 \right) d\mathbf{x}, \tag{3}$$

and $\mathcal{E}_l(\phi)$ denotes the long-range part of $\mathcal{E}(\phi)$

$$\mathcal{E}_l(\phi) = \frac{\alpha}{2} \int_\Omega \int_\Omega G(\mathbf{x} - \mathbf{y}) \left(\phi(\mathbf{x}) - \bar{\phi} \right) \left(\phi(\mathbf{y}) - \bar{\phi} \right) d\mathbf{y} d\mathbf{x}, \tag{4}$$

where G is the Green's function, satisfying $\Delta G(\mathbf{x} - \mathbf{y}) = -\delta(\mathbf{x} - \mathbf{y})$. Here, periodic boundary conditions are assumed and δ is Dirac delta function. By taking a variational derivative, we have

$$\frac{\delta \mathcal{E}_s(\phi)}{\delta \phi} = F'(\phi) - \epsilon^2 \Delta \phi = \mu, \tag{5}$$

$$\frac{\delta \mathcal{E}_l(\phi)}{\delta \phi} = \alpha \int_\Omega G(\mathbf{x} - \mathbf{y}) \left(\phi(\mathbf{y}) - \bar{\phi} \right) d\mathbf{y}. \tag{6}$$

Next, we deduce Eq. (1) by substituting Eqs. (5) and (6) into the mass conserved gradient flow.

$$\phi_t = \Delta \left(\frac{\delta \mathcal{E}_s(\phi)}{\delta \phi} + \frac{\delta \mathcal{E}_l(\phi)}{\delta \phi} \right) = \Delta \mu - \alpha \left(\phi - \bar{\phi} \right). \tag{7}$$

Note that if ν satisfies $-\Delta\nu = \phi - \bar{\phi}$ with the periodic boundary condition, then we can represent $\mathcal{E}_l(\phi)$ as follows [8, 21]:

$$\mathcal{E}_l(\phi) = \frac{\alpha}{2}\int_\Omega \Delta_{\mathbf{x}}\nu(\mathbf{x})\left[\int_\Omega \Delta_{\mathbf{y}}G(\mathbf{x}-\mathbf{y})\nu(\mathbf{y})\,d\mathbf{y}\right]d\mathbf{x} = \frac{\alpha}{2}\int_\Omega |\nabla\nu(\mathbf{x})|^2\,d\mathbf{x}. \tag{8}$$

This form is convenient for the numerical analysis and numerical evaluation. Thus, we can represent the energy functional as

$$\mathcal{E}(\phi) = \int_\Omega \left(F(\phi) + \frac{\epsilon^2}{2}|\nabla\phi|^2 + \frac{\alpha}{2}|\nabla\nu|^2\right)d\mathbf{x}. \tag{9}$$

Differentiate $\mathcal{E}(\phi)$ and $\int_\Omega \phi d\mathbf{x}$ with respect to time, using the periodic boundary condition, we have

$$\begin{aligned}\frac{d}{dt}\mathcal{E}(\phi) &= \int_\Omega \left(F'(\phi)\phi_t + \epsilon^2\nabla\phi\cdot\nabla\phi_t + \alpha\nabla\nu\cdot\nabla\nu_t\right)d\mathbf{x}\\ &= \int_\Omega \left(\left(F'(\phi) - \epsilon^2\Delta\phi\right)\phi_t - \alpha\nu\Delta\nu_t\right)d\mathbf{x}\\ &= \int_\Omega (\mu+\alpha\nu)\,\phi_t\;d\mathbf{x} = -\int_\Omega |\nabla(\mu+\alpha\nu)|^2\,d\mathbf{x} \le 0\end{aligned} \tag{10}$$

and

$$\begin{aligned}\frac{d}{dt}\int_\Omega \phi\;d\mathbf{x} = \int_\Omega \phi_t\;d\mathbf{x} &= \int_\Omega \left(\Delta\mu - \alpha\left(\phi-\bar{\phi}\right)\right)d\mathbf{x}\\ &= \int_{\partial\Omega}\frac{\partial\mu}{\partial\mathbf{n}}\,d\mathbf{s} - \alpha\int_\Omega\left(\phi-\bar{\phi}\right)d\mathbf{x} = 0.\end{aligned} \tag{11}$$

Therefore, the energy is not increased and the mass is conserved in time.

This paper is organized as follows. In Section 2, we present the numerical scheme and prove its mass conservation, solvability, energy dissipation, and stability. In Section 3, a brief numerical solution procedure is given to condense the discussion. Numerical results are described in Section 4 and conclusions are stated in Section 5.

2. Numerical analysis

We present a finite difference scheme for the Ohta–Kawasaki equation. We discretize the equation in a domain $\Omega = [a, b]$. Let M and N be positive integers, $h = (b-a)/M$ be the uniform mesh size, $\Delta t = T/N$ be the uniform time step, and $\Omega_h = \{x_i = (i-0.5)h,\ i = 1, 2, \ldots, M\}$ be the set of cell-centers. Let ϕ_i^n be the approximation of $\phi(x_i, n\Delta t)$ and $\boldsymbol{\phi}^n = (\phi_1^n, \phi_2^n, \ldots, \phi_M^n)$. The periodic boundary condition for $\boldsymbol{\phi}^n$ is implemented as $\phi_0^n = \phi_M^n$ and $\phi_{M+1}^n = \phi_1^n$. We define the discrete differentiation and Laplacian operators as $\nabla_h\phi_{i+\frac{1}{2}}^n = (\phi_{i+1}^n - \phi_i^n)/h$ and $\Delta_h\phi_i^n = (\nabla_h\phi_{i+\frac{1}{2}}^n - \nabla_h\phi_{i-\frac{1}{2}}^n)/h$. For $\boldsymbol{\phi}$ and $\boldsymbol{\psi}$, we define

discrete inner products by

$$\langle \boldsymbol{\phi}, \boldsymbol{\psi} \rangle_h = h \sum_{i=1}^{M} \phi_i \psi_i, \quad (\nabla_h \boldsymbol{\phi}, \nabla_h \boldsymbol{\psi})_h = h \sum_{i=1}^{M} \nabla_h \phi_{i+\frac{1}{2}} \nabla_h \psi_{i+\frac{1}{2}}. \tag{12}$$

We define the discrete norms as $\|\boldsymbol{\phi}\|_h^2 = \langle \boldsymbol{\phi}, \boldsymbol{\phi} \rangle_h$ and $\|\boldsymbol{\phi}\|_\infty = \max_{1 \le i \le M} |\phi_i|$. If the periodic boundary condition for $\boldsymbol{\phi}$ and $\boldsymbol{\psi}$ is assumed, we have a summation by parts, $\langle \Delta_h \boldsymbol{\phi}, \boldsymbol{\psi} \rangle_h = \langle \boldsymbol{\phi}, \Delta_h \boldsymbol{\psi} \rangle_h = -(\nabla_h \boldsymbol{\phi}, \nabla_h \boldsymbol{\psi})_h$.

We denote the matrix version of Δ_h with the periodic boundary condition as

$$\Delta_d = \frac{1}{h^2} \begin{pmatrix} -2 & 1 & & & 1 \\ 1 & -2 & 1 & & \\ & \ddots & \ddots & \ddots & \\ & & 1 & -2 & 1 \\ 1 & & & 1 & -2 \end{pmatrix}. \tag{13}$$

Matrix $-\Delta_d$ is the positive semi-definite with eigenvalues $\lambda_i = \frac{4}{h^2} \sin^2 \frac{(i-1)\pi}{M}$, for $i = 1, 2, \ldots, M$. Let $\mathbf{v}_i$ be the orthonormal eigenvector corresponding to the eigenvalue λ_i. For $\mathbf{X}$ and $\mathbf{Y}$ in $\mathbb{R}^M$, we can represent as $\mathbf{X} = \sum_{i=1}^{M} \alpha_i \mathbf{v}_i$ and $\mathbf{Y} = \sum_{i=1}^{M} \beta_i \mathbf{v}_i$, where $\alpha_i = \langle \mathbf{X}, \mathbf{v}_i \rangle_h$ and $\beta_i = \langle \mathbf{Y}, \mathbf{v}_i \rangle_h$. We define

$$\langle \mathbf{X}, \mathbf{Y} \rangle_{-1,h} := h \sum_{i=2}^{M} \lambda_i^{-1} \alpha_i \beta_i. \tag{14}$$

Note that if $\alpha_1 = 0$ or $\beta_1 = 0$, we have the identity $\langle \mathbf{X}, \mathbf{Y} \rangle_h = \langle -\Delta_d \mathbf{X}, \mathbf{Y} \rangle_{-1,h}$. And, we define the discrete norm $\|\mathbf{X}\|_{-1,h}^2 = \langle \mathbf{X}, \mathbf{X} \rangle_{-1,h}$. Let us define a discrete free energy functional

$$\mathcal{E}^h(\boldsymbol{\phi}^n) = \langle F(\boldsymbol{\phi}^n), \mathbf{1} \rangle_h + \frac{\epsilon^2}{2} (\nabla_h \boldsymbol{\phi}^n, \nabla_h \boldsymbol{\phi}^n)_h + \frac{\alpha}{2} (\nabla_h \boldsymbol{\nu}^n, \nabla_h \boldsymbol{\nu}^n)_h, \tag{15}$$

where $F(\boldsymbol{\phi}^n) = (F(\phi_1^n), F(\phi_2^n), \ldots, F(\phi_M^n))$ and $-\Delta_d \boldsymbol{\nu}^n = \boldsymbol{\phi}^n - \bar{\phi}$ with $\langle \boldsymbol{\nu}^n, \mathbf{1} \rangle_h = 0$. We then separate $\mathcal{E}^h(\boldsymbol{\phi}^n)$ into four parts:

$$\mathcal{E}^{(1)}(\boldsymbol{\phi}^n) = \langle F_e(\boldsymbol{\phi}^n), \mathbf{1} \rangle_h, \qquad \mathcal{E}^{(2)}(\boldsymbol{\phi}^n) = \frac{\epsilon^2}{2} (\nabla_h \boldsymbol{\phi}^n, \nabla_h \boldsymbol{\phi}^n)_h, \tag{16}$$

$$\mathcal{E}^{(3)}(\boldsymbol{\phi}^n) = \langle F_c(\boldsymbol{\phi}^n), \mathbf{1} \rangle_h, \qquad \mathcal{E}^{(4)}(\boldsymbol{\phi}^n) = \frac{\alpha}{2} (\nabla_h \boldsymbol{\nu}^n, \nabla_h \boldsymbol{\nu}^n)_h, \tag{17}$$

where $F_e(\boldsymbol{\phi}) = \boldsymbol{\phi}^2/2$ and $F_c(\boldsymbol{\phi}) = (\boldsymbol{\phi}^4 + 1)/4$. We denote the discrete biharmonic operator as $\Delta_h^2 \phi_i = \Delta_h(\Delta_h \phi_i)$ and usual gradient in $\mathbb{R}^M$ as $\nabla \mathcal{E}^h(\boldsymbol{\phi}) = \left(\mathcal{E}^h(\boldsymbol{\phi})_{\phi_1}, \mathcal{E}^h(\boldsymbol{\phi})_{\phi_2}, \ldots, \mathcal{E}^h(\boldsymbol{\phi})_{\phi_M}\right)$, and we have

$$\nabla \mathcal{E}^h(\boldsymbol{\phi})_i = h \left[(\phi_i)^3 - \phi_i - \epsilon^2 \Delta_h \phi_i + \alpha \nu_i \right]. \tag{18}$$

For more details, the derivations of the last two terms are

$$\mathcal{E}^{(2)}(\boldsymbol{\phi}^n)_{\phi_i} = \epsilon^2 h \left(\nabla_h \boldsymbol{\phi}^n, \nabla_h \boldsymbol{\phi}_{\phi_i}^n \right)_h = -\epsilon^2 h \left\langle \Delta_h \boldsymbol{\phi}^n, \boldsymbol{\phi}_{\phi_i}^n \right\rangle_h = -\epsilon^2 h \Delta_h \phi_i^n, \tag{19}$$

$$\mathcal{E}^{(4)}(\boldsymbol{\phi}^n)_{\phi_i} = \alpha h \left(\nabla_h \boldsymbol{\nu}^n, \nabla_h \boldsymbol{\nu}_{\phi_i}^n \right)_h = -\alpha h \left\langle \boldsymbol{\nu}^n, \Delta_h \boldsymbol{\nu}_{\phi_i}^n \right\rangle_h = \alpha h \nu_i^n. \tag{20}$$

Since $-\Delta_h \boldsymbol{\nu}^n = \boldsymbol{\phi}^n - \bar{\phi}$ and $\langle \boldsymbol{\phi}^n, \mathbf{1} \rangle_h = \bar{\phi}$, we have the useful identity as

$$\Delta_d \left(\nabla \boldsymbol{\nu}^n \right) = \nabla \left(\Delta_d \boldsymbol{\nu}^n \right) = \nabla \left(-\boldsymbol{\phi}^n + \bar{\phi} \right) = -\mathbf{I}. \tag{21}$$

The Hessian of $\mathcal{E}^{(1)}(\boldsymbol{\phi})$, denoted by $\mathbf{H}^{(1)}$, is the Jacobian of $\nabla \mathcal{E}^{(1)}(\boldsymbol{\phi})$ and therefore, it is given by $\mathbf{H}^{(1)} = \nabla^2 \mathcal{E}^{(1)}(\boldsymbol{\phi}) = hI_M$, where I_M is an identity matrix of order M. In the similar manner, Hessian matrices of $\mathcal{E}^{(2)}(\boldsymbol{\phi})$ and $\mathcal{E}^{(3)}(\boldsymbol{\phi})$ are given as $\mathbf{H}^{(2)} = -h\epsilon^2 \Delta_d$ and $\mathbf{H}^{(3)} = 3h \left(\phi_1^2, \phi_2^2, \ldots, \phi_M^2 \right)$. The eigenvalues of $\mathbf{H}^{(1)}$, $\mathbf{H}^{(2)}$, and $\mathbf{H}^{(3)}$ are $\lambda_i^{(1)} = h$, $\lambda_i^{(2)} = h\epsilon^2 \lambda_i$, and $\lambda_i^{(3)} = 3h\phi_i^2$ for $i = 1, 2, \ldots, M$. Note that $\lambda_i^{(1)}$, $\lambda_i^{(2)}$, and $\lambda_i^{(3)}$ are non-negative.

To apply a nonlinear stabilized splitting scheme [11, 12] to the Ohta–Kawasaki model, we split the discrete function as $\mathcal{E}_c^h(\boldsymbol{\phi}^n) = \mathcal{E}^{(2)}(\boldsymbol{\phi}^n) + \mathcal{E}^{(3)}(\boldsymbol{\phi}^n) + \mathcal{E}^{(4)}(\boldsymbol{\phi}^n)$ and $\mathcal{E}_e^h(\boldsymbol{\phi}^n) = \mathcal{E}^{(1)}(\boldsymbol{\phi}^n)$ so that $\mathcal{E}^h(\boldsymbol{\phi}^n) = \mathcal{E}_c^h(\boldsymbol{\phi}^n) - \mathcal{E}_e^h(\boldsymbol{\phi}^n)$, and we obtain

$$\begin{aligned} \frac{\boldsymbol{\phi}^{n+1} - \boldsymbol{\phi}^n}{\Delta t} &= \frac{\Delta_d}{h} \left(\nabla \mathcal{E}_c^h \left(\boldsymbol{\phi}^{n+1} \right) - \nabla \mathcal{E}_e^h \left(\boldsymbol{\phi}^n \right) \right) \\ &= \Delta_d \left(\left(\boldsymbol{\phi}^{n+1} \right)^3 - \boldsymbol{\phi}^n - \epsilon^2 \Delta_d \boldsymbol{\phi}^{n+1} \right) \end{aligned} \tag{22}$$

for $i = 1, 2, \ldots, M$. The numerical system is completed by imposing the periodic boundary condition to $\boldsymbol{\phi}^{n+1}$ and $\boldsymbol{\mu}^{n+1}$. Since $\bar{\phi} = \langle \boldsymbol{\phi}^n, \mathbf{1} \rangle_h$, we have

$$\begin{aligned} \left\langle \boldsymbol{\phi}^{n+1}, \mathbf{1} \right\rangle_h &= \langle \boldsymbol{\phi}^n, \mathbf{1} \rangle_h + \Delta t \left\langle \Delta_h \boldsymbol{\mu}^{n+1}, \mathbf{1} \right\rangle_h - \alpha \Delta t \left\langle \boldsymbol{\phi}^{n+1} - \bar{\phi} \mathbf{1}, \mathbf{1} \right\rangle_h \\ &= \langle \boldsymbol{\phi}^n, \mathbf{1} \rangle_h - \alpha \Delta t \left\langle \boldsymbol{\phi}^{n+1} - \boldsymbol{\phi}^n, \mathbf{1} \right\rangle_h . \end{aligned} \tag{23}$$

The positiveness of α implies the mass conservation $\left\langle \boldsymbol{\phi}^{n+1}, \mathbf{1} \right\rangle_h = \langle \boldsymbol{\phi}^n, \mathbf{1} \rangle_h$.

2.1. Solvability

Here, we construct an appropriate functional of our scheme, and then prove the existence and uniqueness of a solution for the minimizer of the functional. Bearing in mind that we want to have Eq. (22) as the first variation of a functional, we consider the functional $G(\boldsymbol{\phi})$ for $\boldsymbol{\phi}$ satisfying $\langle \boldsymbol{\phi}, \mathbf{1} \rangle_h = \bar{\phi}$

$$G(\boldsymbol{\phi}) = \frac{1}{2\Delta t} \left\| \boldsymbol{\phi} - \boldsymbol{\phi}^n \right\|_{-1,h}^2 + \mathcal{E}_c^h(\boldsymbol{\phi}) - \frac{1}{h} \left\langle \nabla \mathcal{E}_e^h(\boldsymbol{\phi}^n), \boldsymbol{\phi} \right\rangle_h . \tag{24}$$

The first variation of $G(\boldsymbol{\phi})$ is

$$\delta G(\boldsymbol{\phi}; \boldsymbol{\psi}) = \frac{1}{\Delta t} \left\langle \boldsymbol{\phi} - \boldsymbol{\phi}^n, \boldsymbol{\psi} \right\rangle_{-1,h} + \frac{1}{h} \left\langle \nabla \mathcal{E}_c^h(\boldsymbol{\phi}) - \nabla \mathcal{E}_e^h(\boldsymbol{\phi}^n), \boldsymbol{\psi} \right\rangle_h . \tag{25}$$

In addition, the second variation of $G(\boldsymbol{\phi})$ is

$$\begin{aligned} \delta^2 G(\boldsymbol{\phi}; \boldsymbol{\psi}) &= h \left\| \boldsymbol{\psi} \right\|_{-1,h}^2 + \Delta t \left\langle \nabla^2 \mathcal{E}_c^h(\boldsymbol{\phi}) \boldsymbol{\psi}, \boldsymbol{\psi} \right\rangle_h \\ &= h(1 + \alpha \Delta t) \left\| \boldsymbol{\psi} \right\|_{-1,h}^2 + \Delta t \left\langle \left(\mathbf{H}^{(2)} + \mathbf{H}^{(3)} \right) \boldsymbol{\psi}, \boldsymbol{\psi} \right\rangle_h > 0. \end{aligned} \tag{26}$$

Let us consider the critical point $\boldsymbol{\phi}^*$ of $G(\boldsymbol{\phi})$. From Eq. (25), for any $\boldsymbol{\psi}$, we have

$$\delta G(\boldsymbol{\phi}^*;\boldsymbol{\psi}) = \left\langle \frac{\boldsymbol{\phi}^* - \boldsymbol{\phi}^n}{\Delta t} - \frac{\Delta_d}{h}\left(\nabla \mathcal{E}_c^h(\boldsymbol{\phi}^*) - \nabla \mathcal{E}_e^h(\boldsymbol{\phi}^n)\right), \boldsymbol{\psi} \right\rangle_{-1,h} = 0. \tag{27}$$

Strict convexity of $G(\boldsymbol{\phi})$ implies that $\boldsymbol{\phi}^*$ is the unique minimum in H. Furthermore, by substituting $\boldsymbol{\phi}^{n+1}$ for $\boldsymbol{\phi}^*$ into Eq. (27), we have

$$\frac{\phi_i^{n+1} - \phi_i^n}{\Delta t} = \frac{\Delta_h}{h}\left(\nabla \mathcal{E}_c^h(\boldsymbol{\phi}^{n+1})_i - \nabla \mathcal{E}_e^h(\boldsymbol{\phi}^n)_i\right) \tag{28}$$

for $i = 1, 2, \ldots, M$, which is identical to Eq. (22).

2.2. Unconditional gradient stability

We provide a simple proof of the energy dissipation property for the sake of completeness. Suppose that $\boldsymbol{\phi}^{n+1}$ is the solution of Eq. (22) with given $\boldsymbol{\phi}^n$. We begin with introducing the following inequality

$$F\left(\phi_i^{n+1}\right) - F\left(\phi_i^n\right) \le \frac{1}{2}\left(\left(\phi_i^{n+1}\right)^2 - \left(\phi_i^n\right)^2\right)\left(\left(\phi_i^{n+1}\right)^2 - 1\right) \tag{29}$$

using $a^2 - b^2 = 2(a-b)a - (a-b)^2 \le 2(a-b)a$. Now, the energy difference can be manipulated as

$$\begin{aligned}
&\mathcal{E}^h\left(\boldsymbol{\phi}^{n+1}\right) - \mathcal{E}^h\left(\boldsymbol{\phi}^n\right) \\
&\le \frac{1}{2}\left\langle \left(\boldsymbol{\phi}^{n+1}\right)^2 - \left(\boldsymbol{\phi}^n\right)^2, \left(\boldsymbol{\phi}^{n+1}\right)^2 - \mathbf{1} \right\rangle_h \\
&\quad + \epsilon^2 \left\langle \nabla_h\left(\boldsymbol{\phi}^{n+1} - \boldsymbol{\phi}^n\right), \nabla_h \boldsymbol{\phi}^{\boldsymbol{n}} \right\rangle_h + \left\langle \nabla_h\left(\boldsymbol{\nu}^{n+1} - \boldsymbol{\nu}^n\right), \nabla_h \boldsymbol{\nu}^{\boldsymbol{n}} \right\rangle_h \\
&= \left\langle \boldsymbol{\phi}^{n+1} - \boldsymbol{\phi}^n, \left(\boldsymbol{\phi}^{n+1}\right)^3 - \boldsymbol{\phi}^n - \epsilon^2 \Delta \boldsymbol{\phi}^{n+1} + \alpha \boldsymbol{\nu}^{n+1} \right\rangle_h \\
&\quad - \left\langle \left(\boldsymbol{\phi}^{n+1} - \boldsymbol{\phi}^n\right)^2, \frac{1}{2} + \left(\boldsymbol{\phi}^{n+1}\right)^2 \right\rangle_h \\
&\le \Delta t \left\langle \Delta_d \boldsymbol{\mu}^{n+1}, \boldsymbol{\mu}^{n+1} \right\rangle_h \le 0.
\end{aligned} \tag{30}$$

Therefore, we prove the decrease of discrete functional, i.e., $\mathcal{E}^h(\boldsymbol{\phi}^n) \ge \mathcal{E}^h(\boldsymbol{\phi}^{n+1})$, for any time step Δt. Furthermore, we note that the energy dissipation implies unconditional stability following the similar manner in [18]. The decrease of discrete functional $\mathcal{E}^h(\boldsymbol{\phi}^n)$ implies that

$$\mathcal{E}^h(\boldsymbol{\phi}^0) \ge \mathcal{E}^h(\boldsymbol{\phi}^n) \ge \langle F(\boldsymbol{\phi}^n), \mathbf{1} \rangle_h \ge h F(\phi_i^n) = \frac{h}{4}\left(\phi_i^2 - 1\right)^2 \tag{31}$$

for any i. We then have the pointwise boundedness of the numerical solution as $\|\boldsymbol{\phi}^n\|_\infty \le \sqrt{1 + 2\sqrt{\mathcal{E}^h(\boldsymbol{\phi}^0)/h}}$ for all n. Therefore, we deduce that the proposed numerical scheme is unconditionally stable.

3. Numerical solution

We recall the proposed numerical method (22) to solve the Ohta–Kawasaki equation

$$\frac{\phi_i^{n+1}-\phi_i^n}{\Delta t} = \Delta_h \mu_i^{n+1} - \alpha\left(\phi_i^{n+1}-\bar{\phi}\right), \tag{32}$$

$$\mu_i^{n+1} = \left(\phi_i^{n+1}\right)^3 - \phi_i^n - \epsilon^2 \Delta_h \phi_i^{n+1}, \tag{33}$$

where $\bar{\phi} = \langle \boldsymbol{\phi}^n, \mathbf{1}\rangle_h$ for $i = 1, 2, \ldots, M$ and $n = 0, 2, \ldots, N-1$.

We use a multigrid method to solve the discretized system (32) and (33). To condense the discussion, we describe only the nonlinear system for the multigrid method.

$$(1+\alpha\Delta t)\,\phi_i^{n+1} - \Delta_h \mu_i^{n+1} = \phi_i^n + \alpha\Delta t\bar{\phi}, \tag{34}$$

$$-\left(\phi_i^{n+1}\right)^3 + \epsilon^2\Delta_h\phi_i^{n+1} + \mu_i^{n+1} = -\phi_i^n \tag{35}$$

for $i = 1, 2, \ldots, M$. Because of the nonlinearity for ϕ_i^{n+1}, we linearized $\left(\phi_i^{n+1}\right)^3$ at $\phi_i^{n,k}$

$$\left(\phi_i^{n+1}\right)^3 \approx \left(\phi_i^{n,k}\right)^3 + 3\left(\phi_i^{n,k}\right)^2\left(\phi_i^{n+1}-\phi_i^{n,k}\right). \tag{36}$$

We then consider the nonlinear iterative method as

$$(1+\alpha\Delta t)\phi_i^{n,k+1} - \Delta_h\mu_i^{n,k+1} = \phi_i^n + \alpha\Delta t\bar{\phi}, \tag{37}$$

$$-3\left(\phi_i^{n,k}\right)^2\phi_i^{n,k+1} + \epsilon^2\Delta_h\phi_i^{n,k+1} + \mu_i^{n,k+1} = -\phi_i^n - 2\left(\phi_i^{n,k}\right)^3, \tag{38}$$

where $\phi_i^{n,0} = \phi_i^n$. A pointwise Gauss–Seidel relaxation is used as the smoother in the multigrid method. If the l_2 norm of the consecutive error $\|\boldsymbol{\phi}^{n,k+1} - \boldsymbol{\phi}^{n,k}\|_2$ is less than 10^{-9}, we have $\phi_i^{n+1} = \phi_i^{n,k+1}$. For more details, we refer to [17, 26].

4. Numerical results

First, we consider the local Fourier analysis for the nonlinear scheme and estimate the numerical convergence factor. Next, we confirm the numerical accuracy of the proposed scheme for solving the Ohta–Kawasaki equation. Finally, we perform numerical experiments for demonstrate the mass conservation, energy dissipation, and unconditional stability.

4.1. Local Fourier analysis

To analyze the behavior of the multigrid method, we linearize the nonlinear scheme and perform a local Fourier analysis (LFA), which is introduced by Brandt [4]. In LFA, a current approximation and its residual are represented by a linear combination of Fourier modes. A unitary basis of the Fourier modes is defined by $e^{i\theta x/h}$ where $\theta \in (-\pi, \pi]$ is called Fourier frequency.

Since the performance of the multigrid method depends strongly on the smoother, we analyze the smoother to evaluate its effect on the Fourier components using LFA [20]. LFA allows us to obtain quantitative estimates of the performance of multigrid method. Although LFA was originally designed for the linear problem, it can also be employed for the analysis of the nonlinear problem by using freezing coefficients [26].

Let ϕ_i^n and μ_i^n be solutions of the discrete Ohta–Kawasaki equation (34) and (35). After linearizing the nonlinear term $\left(\phi_i^{n+1}\right)^3 = \beta\phi_i^{n+1}$, where β is a freezing constant for $(\phi^m)^2$. Substituting μ_i^n into Eq. (34), it becomes

$$L_h\phi_i^n = f_i^n, \tag{39}$$

where

$$\begin{aligned} L_h\phi_i^n = \phi_i^{n+1} &- \beta\frac{\Delta t}{h^2}\left(\phi_{i-1}^{n+1} - 2\phi_i^{n+1} + \phi_{i+1}^{n+1}\right) \\ &+ \epsilon^2\frac{\Delta t}{h^4}\left(\phi_{i-2}^{n+1} - 4\phi_{i-1}^{n+1} + 6\phi_i^{n+1} - 4\phi_{i+1}^{n+1} + \phi_{i+2}^{n+1}\right) + \alpha\Delta t\phi_i^{n+1} \end{aligned} \tag{40}$$

and

$$f_i^n = \phi_i^n - \Delta_h\phi_i^n + \alpha\bar{\phi}. \tag{41}$$

For the Gauss–Seidel iteration with a lexicographic ordering of the grid points applied to the above equation, we have the following operator decomposition:

$$L_h^+\phi_i = \phi_i - \beta\frac{\Delta t}{h^2}\left(\phi_{i-1} - 2\phi_i\right) + \epsilon^2\frac{\Delta t}{h^4}\left(\phi_{i-2} - 4\phi_{i-1} + 6\phi_i\right) + \alpha\Delta t\phi_i, \tag{42}$$

$$L_h^-\phi_i = -\beta\frac{\Delta t}{h^2}\phi_{i+1} + \epsilon^2\frac{\Delta t}{h^4}\left(-4\phi_{i+1} + \phi_{i+2}\right). \tag{43}$$

Now, the Gauss–Seidal iterative method can be written as

$$L_h^+\boldsymbol{\phi}^{n,m+1} + L_h^-\boldsymbol{\phi}^{n,m} = \boldsymbol{f}^n, \tag{44}$$

where $\boldsymbol{\phi}^{n,m+1}$ is the new approximation after the relaxation step, given the old approximation $\boldsymbol{\phi}^{n,m}$ for $\boldsymbol{\phi}^{n+1}$. Subtracting Eq. (44) from the discrete equation $L_h\boldsymbol{\phi}^{n+1} = \boldsymbol{f}^n$ and defining $\boldsymbol{\psi}^{n,m+1} = \boldsymbol{\phi}^{n+1} - \boldsymbol{\phi}^{n,m+1}$ and $\boldsymbol{\psi}^{n,m} = \boldsymbol{\phi}^{n+1} - \boldsymbol{\phi}^{n,m}$, we obtain the equation

$$L_h^+\boldsymbol{\psi}^{n,m+1} + L_h^-\boldsymbol{\psi}^{n,m} = \mathbf{0}, \tag{45}$$

or, equivalently,

$$\boldsymbol{\psi}^{n,m+1} = S_h\boldsymbol{\psi}^{n,m}, \tag{46}$$

where we denote $S_h = -\left(L_h^+\right)^{-1}L_h^-$ as the resulting smoothing operator. Applying L_h^+ and L_h^- to the formal eigenfunctions $e^{i\theta x/h}$, we obtain

$$L_h^+e^{i\theta x/h} = \hat{L}_h^+e^{i\theta x/h}, \tag{47}$$

$$L_h^-e^{i\theta x/h} = \hat{L}_h^-e^{i\theta x/h}, \tag{48}$$

where $\hat{L}_h^+$ and $\hat{L}_h^-$ are the eigenvalues of the operators L_h^+ and L_h^-, respectively,

$$\hat{L}_h^+(\theta) = 1 - \beta\frac{\Delta t}{h^2}\left(e^{-i\theta} - 2\right) + \epsilon^2\frac{\Delta t}{h^4}\left(e^{-2i\theta} - 4e^{-i\theta} + 6\right) + \alpha\Delta t, \tag{49}$$

$$\hat{L}_h^-(\theta) = -\beta\frac{\Delta t}{h^2}e^{i\theta} + \epsilon^2\frac{\Delta t}{h^4}\left(-4e^{i\theta} + e^{2i\theta}\right). \tag{50}$$

The amplification factor of the relaxation scheme is

$$\hat{S}_h(\theta) = -\frac{\hat{L}_h^-(\theta)}{\hat{L}_h^+(\theta)}. \tag{51}$$

Figure 1 displays the absolute value of amplification factor with respect to the Fourier frequency mode. We consider two examples of $\beta = 0$ and $\beta = 0.25$, and other parameters are $\Delta t = 0.1h$, $\epsilon = 0.01$, and $\alpha = 100$. In the figure, we observe the standard smoothing property of the relaxation scheme which makes it effective at eliminating the high-frequency, while leaving the low-frequency relatively unchanged. By the restriction procedure from the fine grid to coarse grid, a mode becomes more oscillatory in the view of the coarse grid. Therefore, the relaxation in the coarse grid will be more effective. For more interested readers for the multigrid method, we refer to [26].

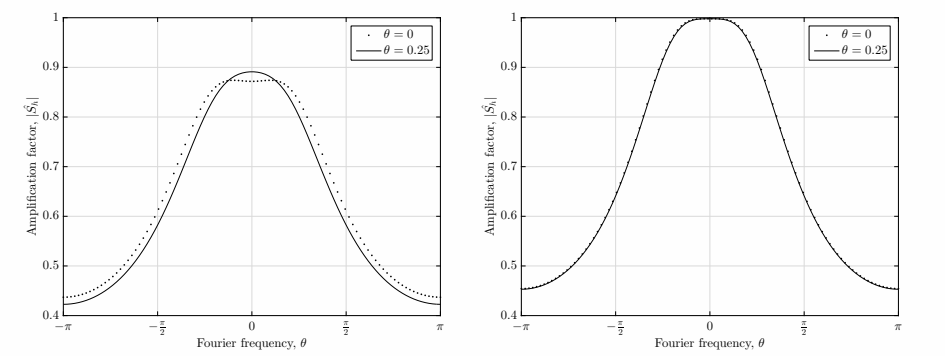

(a) $h = 1/64$ (b) $h = 1/256$

FIGURE 1. Amplification factor via the Fourier frequency.

Now, we define the high frequency smoothing (HFS) factor as

$$\mu_{loc}(S_h) = \left\{\left|\hat{S}_h(\theta)\right| : \frac{\pi}{2} \le |\theta| \le \pi\right\}. \tag{52}$$

HFS factor can be a measurement of the multigrid method by assuming that the coarse grid operators are ideal and annihilate the low frequency error components.

The convergence factor is estimated numerically using our nonlinear code with the parameters $\epsilon = 0.01$, the mesh-dependent time step $\Delta t = 0.1h$ and

initial conditions

$$\phi^0(x) = \begin{cases} 0.0 + 0.01\cos(0.5\pi x/h), & \beta = 0, \\ 0.5 + 0.01\cos(0.5\pi x/h), & \beta = 0.25. \end{cases} \tag{53}$$

We define a defect reduction factor as $q^{(m)} = \|d_h^{m+1}\|/\|d_h^m\|$, where d_h^m are the defect for $m = 1, 2, \ldots$. Here, the defect is defined as $d_h^m = f_h^n - L_h\phi_h^m$. We numerically estimate a convergence factor as an averaged defect reduction factor

$$\hat{q}^{(m)} = \sqrt[m]{q^{(m)}q^{(m-1)}\cdots q^{(1)}}. \tag{54}$$

We measure the $V(m,n)$-cycle convergence factors, where m and n are the numbers of pre-smoothing and post-smoothing, with different grid sizes. We focus on $(1,1)$ as these yield the most efficient algorithms. In addition, we set $\alpha = 100$ and consider $\beta = 0$ and $\beta = 0.25$, where the values correspond to linearization in the stable ranges of the evolution. Note that $\sqrt{V(1,1)}$-cycle means the square root of $V(1,1)$-cycle convergence factor.

Tables 1 and 2 show HFS factors and measured $\sqrt{V(1,1)}$-cycle convergence factors with different mesh sizes and β. The numerically measured convergence factors are uniformly bounded below the theoretical estimate 0.8024 with increasing resolution.

TABLE 1. HFS factors and convergence factors with different mesh size, $\alpha = 100$, $\beta = 0$, $\Delta t = 0.1h$, and $h = 1/M$.

Case	$M = 16$	$M = 32$	$M = 64$	$M = 128$
μ_{loc}	0.1389	0.4586	0.6149	0.6402
$\sqrt{V(1,1)}$-cycle	0.2090	0.3563	0.4437	0.5317
Case	$M = 256$	$M = 512$	$M = 1024$	$M = 2048$
μ_{loc}	0.6435	0.6439	0.6439	0.6439
$\sqrt{V(1,1)}$-cycle	0.5639	0.5852	0.5964	0.6114

TABLE 2. HFS factors and convergence factors with different mesh size, $\alpha = 100$, $\beta = 0.25$, $\Delta t = 0.1h$, and $h = 1/M$.

Case	$M = 16$	$M = 32$	$M = 64$	$M = 128$
μ_{loc}	0.2102	0.4258	0.5823	0.6302
$\sqrt{V(1,1)}$-cycle	0.3136	0.3819	0.4550	0.5022
Case	$M = 256$	$M = 512$	$M = 1024$	$M = 2048$
μ_{loc}	0.6409	0.6432	0.6438	0.6439
$\sqrt{V(1,1)}$-cycle	0.5448	0.5751	0.5839	0.6077

4.2. Convergence test

We demonstrate the time and space convergence rate for the proposed scheme. The initial state for the test is $\phi(x,0) = 0.15 + 0.01\cos(10\pi x) + 0.02\cos(5\pi x)$ in a domain $\Omega = [0,1]$. All simulations are run up to time $T_f = 0.01$ with $\epsilon = 0.015$ and $\alpha = 100$. To calculate the convergence rate in space, we perform a number of simulations on a set of increasing finer grids. The numerical solutions are computed on the grids $h = 1/2^n$ for $n = 6,7,8,9$ with a fixed time step $\Delta t =$ 1E-4. We define the error of a grid to be the l_2-norm of the difference with the next finer grid, $e_{hi} = \phi_{hi} - \frac{1}{2}\left(\phi_{\frac{h}{2}2i-1} + \phi_{\frac{h}{2}2i}\right)$. The rate of the convergence is defined as the ratio of successive errors as $\log_2\left(\|e_h\|/\|e_{\frac{h}{2}}\|\right)$. Table 3 shows the error and rates of convergence. The results suggest that the scheme is second-order accurate in space.

TABLE 3. Errors and convergence rates in space.

case	64–128	rate	128–256	rate	256–512	rate	512–1024
l_2-error	2.22E-2	2.17	4.81E-3	2.03	1.18E-3	2.01	2.93E-4

Next, to estimate the convergence rate in time, we execute a number of simulations with different time steps. The numerical solutions are computed with the time steps $\Delta t = T_f/2^m$ for $m = 8,9,10,11$ with a fixed space step $h = 1/2^7$. We define the error of a grid to be the l_2-norm of the difference with the smaller time step, $e_{\Delta t} = \phi_{\Delta t} - \phi_{\frac{\Delta t}{2}}$. Table 4 shows the error and rates of convergence. The results suggest that the scheme is first-order accurate in time.

TABLE 4. Errors and convergence rates in space.

case	$T_f/2^8$	rate	$T_f/2^9$	rate	$T_f/2^{10}$	rate	$T_f/2^{11}$
l_2-error	9.39E-3	1.20	4.10E-3	1.08	1.93E-3	1.03	9.43E-4

4.3. Mass conservation and energy dissipation

Figure 2 shows the energy and solution evolutions with an initial state $\phi(x,0) = 0.15 + 0.01 \cdot \mathrm{rand}(x)$, where $\mathrm{rand}(x)$ is a random value between -1 and 1. We take the simulation parameters as $\Omega = [0,1]$, $\epsilon = 0.01$, $h = 1/512$, $\Delta t = 0.0001$, and $\alpha = 100$. In Fig. 2(a), we illustrate the discrete total energy and average concentration of numerical solutions. The energy is not increased and the average concentration is conserved. And, Fig. 2(b) draws the solutions at three different times.

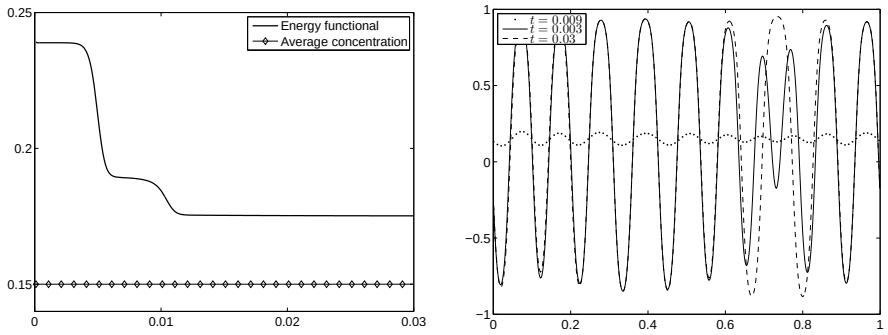

(a) (b)

FIGURE 2. (a) Non-dimensional discrete total energy $\mathcal{E}^h(\boldsymbol{\phi}^n)/\mathcal{E}^h(\boldsymbol{\phi}^0)$ (solid line) and the average concentration $\langle \boldsymbol{\phi}^n, \mathbf{1} \rangle_h$ (diamond). (b) Solution profiles at three different times

4.4. Unconditional stability test

We simulate the numerical test to confirm the unconditional stability of the proposed scheme. We use the initial state $\phi(x, 0) = 0.01\text{rand}(x)$ in $\Omega = [0, 1]$. The parameter $\epsilon = 0.01$, $\alpha = 100$, and $h = 1/512$ are used with three different time steps $\Delta t = 0.01$, 1, and 100. Figure 3 shows that the solutions are not blow up even we use large time steps.

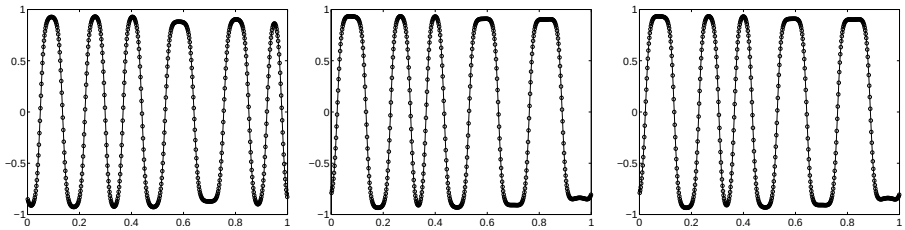

(a) $\Delta t = 0.01$ (b) $\Delta t = 1$ (c) $\Delta t = 100$

FIGURE 3. Snapshots after ten iterations with different time steps

5. Conclusions

We proposed an unconditionally stable scheme for the Ohta–Kawasaki model based on the finite difference method. We then proved the mass conservation, solvability, energy dissipation, and unconditionally gradient stability. And, these properties was confirmed through numerical experiments.

References

[1] M. Bahiana and Y. Oono, *Cell dynamical system approach to block copolymers*, Phys. Rev. A **41** (1990), 6763–6771.

[2] J. W. Barrett, J. F. Blowey, and H. Garcke, *Finite Element Approximation of the Cahn–Hilliard Equation with Degenerate Mobility*, SIAM J. Numer. Anal. **37** (1999), no. 1, 286–318.

[3] F. S. Bates and G. H. Fredrickson, *Block copolymers-designer soft materials*, Phys. Today. **37** (1999), 32–38.

[4] A. Brandt, *Multi-level adaptive solutions to boundary-value problems*, Math. Comp. **31** (1977), no. 138, 333–390.

[5] J. W. Cahn and J. E. Hilliard, *Free energy of a nonuniform system. I. Interfacial free energy*, J. Chem. Phys. **28** (1958), 258–267.

[6] L. Q. Chen and J. Shen, *Applications of semi-implicit Fourier-spectral method to phase field equations*, Comput. Phys. Commun. **108** (1998), 147–158.

[7] R. Choksi, M. Maras, and J. F. Williams, *2D phase diagram for minimizers of a Cahn–Hilliard functional with long-range interactions*, SIAM J. Appl. Dyn. Syst. **10** (2011), no. 4, 1344–1362.

[8] R. Choksi, M. A. Peletier, and J. F. Williams, *On the phase diagram for microphase separation of diblock copolymers: an approach via a nonlocal Cahn–Hilliard functional*, SIAM J. Appl. Math. **69** (2009), no. 6, 1712–1738.

[9] F. Drolet and G. H. Fredrickson, *Combinatorial screening of complex block copolymer assembly with self-consistent field theory*, Phys. Rev. Lett. **83** (1999), 4317–4320.

[10] Q. Du and R. A. Nicolaides, *Numerical analysis of a continuum model of phase transition*, SIAM J. Numer. Anal. **28** (1991), no. 5, 1310–1322.

[11] D. J. Eyre, *An unconditionally stable one-step scheme for gradient systems*, Unpublished article, http://www.math.utah.edu/∼eyre/research/methods/stable.ps (1998).

[12] ———, *Unconditionally gradient stable time marching the Cahn–Hilliard equation*, Computational and mathematical models of microstructural evolution (San Francisco, CA, 1998), 39–46, Mater. Res. Soc. Sympos. Proc., 529, MRS, Warrendale, PA, 1998.

[13] D. Furihata, *A stable and conservative finite difference scheme for the Cahn–Hilliard Equation*, Numer. Math. **87** (2001), no. 4, 675–699.

[14] H. Gómez, V. M. Calo, Y. Bazilevs, and T. J. Hughes, *Isogeometric analysis of the Cahn–Hilliard phase-field model*, Comput. Methods Appl. Mech. Engrg. **197** (2008), no. 49-50, 4333–4352.

[15] Z. Guan, C. Wang, and S. M. Wise, *A convergent convex splitting scheme for the periodic nonlocal Cahn-Hilliard equation*, Numer. Math. **128** (2014), no. 2, 377–406.

[16] D. Jeong, J. Shin, Y. Li, Y. Choi, J. H. Jung, S. Lee, and J. S. Kim, *Numerical analysis of energy-minimizing wavelengths of equilibrium states for diblock copolymers*, Curr. Appl. Phys. **14** (2014), 1263–1272.

[17] J. S. Kim, *A numerical method for the Cahn–Hilliard equation with a variable mobility*, Commun. Nonlinear Sci. Numer. Simul. **12** (2007), no. 8, 1560–1571.

[18] ———, *Phase-field models for multi-component fluid flows*, Commun. Comput. Phys. **12** (2012), no. 3, 613–661.

[19] J. S. Kim and H. O. Bae, *An unconditionally gradient stable adaptive mesh refinement for the Cahn–Hilliard equation*, J. Korean Phys. Soc. **53** (2008), 672–679.

[20] J. S. Kim, K. Kang, and J. S. Lowengrub, *Conservative multigrid methods for Cahn–Hilliard fluids*, J. Comput. Phys. **193** (2004), no. 2, 511–543.

[21] Y. Nishiura and I. Ohnishi, *Some mathematical aspects of the micro-phase separation in diblock copolymers*, Phys. D **84** (1995), no. 1-2, 31–39.

[22] T. Ohta and K. Kawasaki, *Equilibrium morphology of block copolymer melts*, Macromol. **19** (1986), 2621–2632.

[23] M. Pinna and A. V. Zvelindovsky, *Large scale simulation of block copolymers with cell dynamics*, Eur. Phys. J. B **85** (2012), 1–18.
[24] J. Qin, G. S. Khaira, Y. Su, G. P. Garner, M. Miskin, H. M. Jaeger, and J. J. de Pablo, *Evolutionary pattern design for copolymer directed self-assembly*, Soft Matter **9** (2013), 11467–11472.
[25] J. Shin, Y. Choi, and J. S. Kim, *An unconditionally stable numerical method for the viscous Cahn–Hilliard equation*, Discret. Contin. Dyn. Syst. Ser. B **19** (2014), no. 6, 1737–1747.
[26] U. Trottenberg, C. Oosterlee, and A. Schüller, *Multigrid*, Academic press, London, 2001.

Junseok Kim
Department of Mathematics
Korea University
Seoul 136-713, Korea
E-mail address: cfdkim@korea.ac.kr

Jaemin Shin
Institute of Mathematical Sciences
Ewha W. University
Seoul 120-750, Korea
E-mail address: jmshin@ewha.ac.kr